World Academy of Science, Engineering and Technology
International Journal of Bioengineering and Life Sciences
Vol:10, No:12, 2016

Apoptotic Induction Ability of Harmalol and Its Binding: Biochemical and Biophysical Perspectives

Kakali Bhadra

***Abstract*—**Harmalol administration caused remarkable reduction in proliferation of $HepG_2$ cells with GI_{50} of 14.2 μM, without showing much cytotoxicity in embryonic liver cell line, WRL-68. Data from circular dichroism and differential scanning calorimetric analysis of harmalol-CT DNA complex shows conformational changes with prominent CD perturbation and stabilization of CT DNA by 8 ºC. Binding constant and stoichiometry was also calculated using the above biophysical techniques. Further, dose dependent apoptotic induction ability of harmalol was studied in $HepG_2$ cells using different biochemical assays. Generation of ROS, DNA damage, changes in cellular external and ultramorphology, alteration of membrane, formation of comet tail, decreased mitochondrial membrane potential and a significant increase in Sub G_o/G_1 population made the cancer cell, $HepG_2$, prone to apoptosis. Up regulation of p53 and caspase 3 further indicated the apoptotic role of harmalol.

***Keywords*—**Apoptosis, beta carboline alkaloid, comet assay, cytotoxicity, ROS.

I. Introduction

PLANT alkaloids as chemotherapeutic agents isolated so far have been reported to have remarkable anti-cancer applications [1]-[4], and consequently, there is growing interest in the search for anti-cancer drugs with high efficacy, low toxicity and minimum side effects. However, most of the chemotherapeutic agents due to their rather non-selective nature and dose limiting toxicity, use is often restricted. As a result, search for newer drugs having greater potential and suitability for use become necessary. Our previous investigation showed that beta carboline plant alkaloid, harmalol, is an excellent intercalator preferring hetero G/C sequence [5], [6]. Recently, we further showed its RNA binding ability [7]. Harmalol, which was originally isolated from plants like *Peganum harmala* L. and *Banisteriopsis caapi*, has been reported to have several pharmacological, neurophysiological and biochemical activities [8]-[11] as well as *in vivo* and *in vitro* chemopreventive action against different cancer cell line [12]-[14], but its detail apoptotic effect on human cancer cell line has not yet been studied. Inspired by these results, in the present investigation we elucidate, harmalol inducing apoptotic effects in $HepG_2$ cells and consequently study the stabilization, binding and conformational changes in CT DNA using different biochemical and biophysical techniques. Further, event like ROS generation and cell cycle arrests were also accompanied in the harmalol induced apoptosis. The advantage of natural products over synthetic compounds is their abundance in the nature and low toxicity, and in this respect, alkaloids have been one of the most potential and promising pool of small molecules. A complete understanding of these aspects will enable the researchers in future to develop more potent drug as therapeutic agent, to initiate better diagnostic studies for biomedical applications.

Kakali Bhadra is with the Department of Zoology, University of Kalyani, 741235, India (e-mail: kakali_bhadra2004@yahoo.com).

II. Materials and Methods

A. Biochemicals

Harmalol was obtained from Sigma-Aldrich (St. Louis, MO, USA) and the purity was confirmed as done earlier [5], [6]. Its concentration was determined using molar extinction coefficient value of 19,000 M^{-1} cm^{-1} at 371 nm. Double stranded calf thymus DNA (CT DNA) was also obtained from Sigma—Aldrich. Concentration was determined using the molar extinction coefficient (ε) of 6600 M^{-1} cm^{-1} at 260 nm. Harmalol and CT DNA was dissolved in 15 mM Citrate–Phosphate (CP) buffer of pH 6.8.

B. Cell Lines and Culture Conditions

Five different human cell lines *viz.* HeLa (cervical carcinoma), MDA-MB-231 (breast carcinoma), A549 (lung carcinoma), $HepG_2$ (liver epitheloid carcinoma) and WRL-68 (normal hepatic cells) were chosen, obtained from National Centre for Cell Science, Pune. Cells were grown in DMEM supplemented with 10% heat inactivated fetal bovine serum (FBS) and 1% antibiotic–antimycotic, in a humidified atmosphere at 37 ºC with 5% CO_2.

C. Cell Viability Test: MTT Assay

We tested the percentage of cell viability and calculated the GI_{50} (50% growth inhibition) values for the above mentioned cell lines by MTT (1 mg/ml of the tetrazolium dye and 3-(4,5-dimethylthiazol-2-yl)-2,5-diphenyltetrazolium bromide dissolved in phosphate buffer saline, pH 7.4) assay as reported earlier [15].

D. LDH Assay

$HepG_2$ cells were seeded in six-well plates at a density of 2×10^4 cells/well and treated with harmalol of 7, 14 and 21 μM concentrations at 37 ºC for 48 hrs. LDH activity was assessed using a standardized kinetic determination kit (Coral, India).

E. FITC-Annexin V/PI FCM Double Staining

Double staining for FITC (fluorescein isothiocyanate) - Annexin V binding and for cellular DNA using PI (propidium iodide) FCM (flow cytometry) was performed as described by [16].

F. Fluorescence Microscopy

For the identification of nuclear changes such as chromatin condensation, nuclear fragmentation and MMP (mitichrondrial membrane potential) alteration, cells were visualized using a fluorescence microscope (Olympus). DAPI, a blue fluorescent stain, that preferentially stains nuclei (apoptotic or viable). Briefly, cells were plated on coverslips at 2×10^4 /well in a six-well plate for 48 h before treatment. Cells were then stained for 15 min with DAPI (5 μM) at room temperature and mounted on coverslips for observation.

G. Scanning Electron Microscopy (SEM)

To study the external morphology of cell, they were first fixed in glutaraldehyde and dehydrated through a graded series of ethanol. Subsequently, they were cleaned in tetrachloromethane, air-dried and coated with gold in IB2 ION COATER and observed using S530 Hitachi scanning electron microscope.

H. Transmission Electron Microscopy (TEM)

Cultured materials were centrifuged at 3000 rpm for 4-5 min and discarded the supernatant.

The pellet was suspended in 0.1 M phosphate buffer (pH 7.4) dispersed and centrifuged. The pellet was resuspended and fixed in a mixture of 2% paraformaldehyde and 2.5% glutaraldehyde in buffer for 3-4 h at 4 ºC. Centrifuged for 10 min at 4 ºC and the supernatant were discarded. The samples were finally observed using TECNAI 200KV TEM (Fei Electron Optics), 35 mm photography system from All India Institute of Medical Science, N. Delhi.

I. Estimation of DNA Damage

Comet assay was performed on isolated $HepG_2$ cells by single cell gel electrophoresis as reported by Morley *et al.* [17] and examined under fluorescence microscope. The extent of DNA damage was determined by measuring the comet tail length using the software Casp. *2.10 Cell cycle inhibition analysis*

$HepG_2$ cells were grown at a density of 2×10^5 cells/ml in 70 mm culture plate and treated with different concentrations of harmalol (7, 14, 21 μM) for 48 h. The other experimental protocol was followed as reported earlier [15].

J. RT-PCR Analysis

Equal amounts of total RNA, extracted with RNA express reagent (Himedia, Mumbai, India), were reverse transcribed and then subjected to PCR with enzymes and reagents of the reverse transcription system (Chromous) using Techine PCR system (Staffordshire, UK). Sequences of primers used in the study are given in Table I.

K. Generation of ROS and Its Quantification by FACS

Cells (2×10^5) were treated with harmalol at GI_{50} concentration of 14.2 μM for 12, 24 and 48 h and the levels of intracellular H_2O_2 were assessed by flow cytometry after incubating with DCFH-DA (20 μM) (dichloro fluoroscene diacetate) for 30 min at 37 ºC. For inhibition of ROS generation, cells were pretreated with NAC (N-acetyl cysteine) (10 mM) for 30 min before harmalol treatment.

L. Circular Dichroism (CD) Studies

CD spectra were recorded on a Jasco J815 spectropolarimeter (Jasco International Co. Ltd.) attached with a temperature controller and programmer (model PFD 425 L/15) and the experimental parameters were selected as reported earlier [5], [6].

M.Differential Scanning Calorimetry (DSC)

DSC experiments were done on a Microcal VP-differential scanning calorimeter (MicroCal, Inc., Northampton, MA, USA) and used to calculate the binding constant, as reported earlier [18].

N. UV Optical Melting Study

Melting curves were recorded on a Jasco V-630 unit equipped with the peltier controlled Jasco PAC-743 model accessory (Jasco International Co. Ltd. Tokyo, Japan).

III. Results

A. Apoptotic Parameters of Harmalol in $HepG_2$ Cells

To evaluate the efficacy of harmalol (Fig. 1 (A)) on different human cancer cell line *viz*. HeLa, MDA-MB-231, A549, and $HepG_2$, the alkaloid was tested for its cytotoxicity using the MTT assay. After 48 h treatment, it was found that among the above four cell lines, harmalol showed highest degree of concentration-dependent increase in growth inhibition in $HepG_2$ cell line, having GI_{50} value of 14.2 μM (Fig. 1 (B)). However, it exhibited minimal effect (8.5 ± 0.5% apoptosis) on human embryonic liver cell lines, WRL-68, even at a concentration of 55 μM. Beyond this concentration, the alkaloid does not obey the Beer-Lambert's law, hence could not proceed. To further characterize harmalol-induced $HepG_2$ cell death, the LDH assay emphasizing on apoptotic index parameters were compared in both treated and controlled (untreated) cells and observed to be 3.7±1.1% necrotic, 58.5±1.2% apoptotic and 37.8±1.0% viable in treated cell line, where as in controlled cell line, 4.8±1.2%, 11.2 ±0.9% and 84.0±2.1% necrotic, apoptotic and viability, respectively, was observed (Fig. 1 (C)). The morphology of treated and untreated cells as observed by SEM, have been shown in Fig. 1 (D). The morphological changes observed were cell rounding, cytoplasmic blebbing, shrinkage as well as irregularities in cell contour and size in harmalol treated, whereas, in untreated cell line, the cells remain spread out without any sign of irregularities in cell contour and size. Furthermore, ultramorphological study by TEM (Fig. 1 (E)), which is considered the gold standard to confirm apoptosis, further revealed some early and late apoptotic features like nucleolous fragmentation, cytoplasmic blebbing and formation of phagolysomal complex.

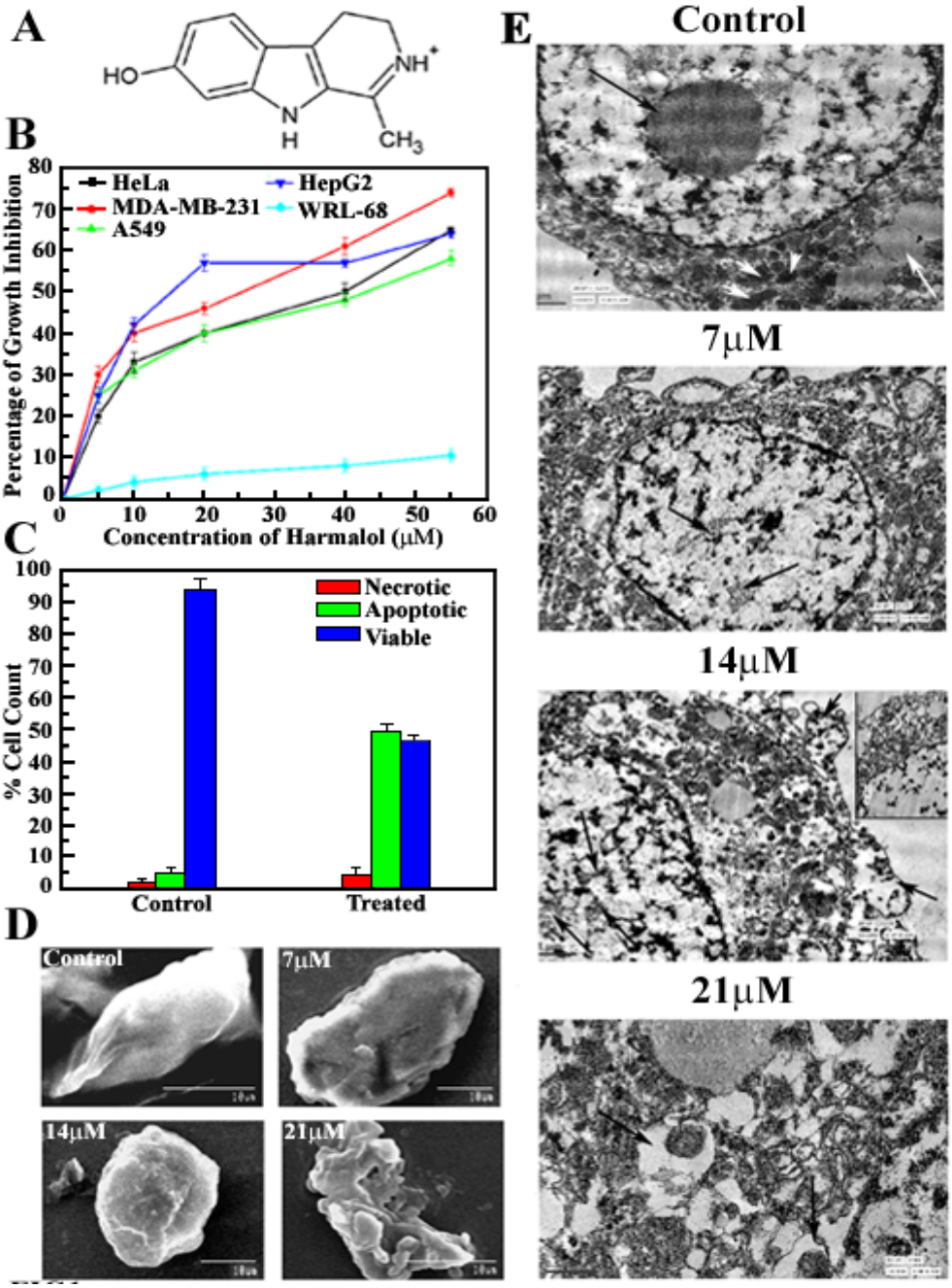

Fig. 1 (A) Chemical structure of harmalol. (B) Percentage growth inhibition of HeLa, MDA-MB-231, A549, $HepG_2$ and WRL-68 cells following treatment with harmalol of varying concentrations (5, 10, 20, 40 and 55 μM) for 48 h. Data are statistically analyzed with ANOVA test (*P< 0.05 vs. solvent control). (C) LDH assay, performed after harmalol treatment. (D) Changes in cell morphology and apoptotic index parameters as observed using SEM. (E) TEM of: untreated $HepG_2$ cell showing enlarge nucleolous, numerous intact mitochondria and lipid droplets, cell after treatment with harmalol at GI_{25} showing sign of nucleolous fragmentation, cell after treatment with harmalol at GI_{50} showing sign of blebs at the cell surface with further progress of nucleolous fragmentation (inset) and cell after treatment with harmalol at GI_{75} showing sign of phagolysosome formation with disorganized cytoplasmic organelles. (Positive changes marked with arrows)

Apoptotic $HepG_2$ cells were also characterized by the formation of comet tails, indicative of DNA damage (Fig. 2 (A)). The results showed more DNA strand breaks constituting of 59±4.3% DNA damage (longest tail length) with the treatment of harmalol at 21 μM of concentration and least damage of DNA (1.6±0.9%) with lowest concentration of 7 μM (Fig. 2 (B), Table II). In addition, $HepG_2$ cells with DAPI staining revealed a significant increase in oligonucleosomal fragmentation and nuclear condensation in harmalol treated cells with increasing doses (Fig. 2 (C)). Furthermore, as evident in DNA gel electrophoresis of harmalol treated cell (Fig. 2 (D)), apoptotic hallmark of chromosomal DNA laddering was clearly evident in $HepG_2$ treated with different doses of the alkaloid as compared to untreated cells.

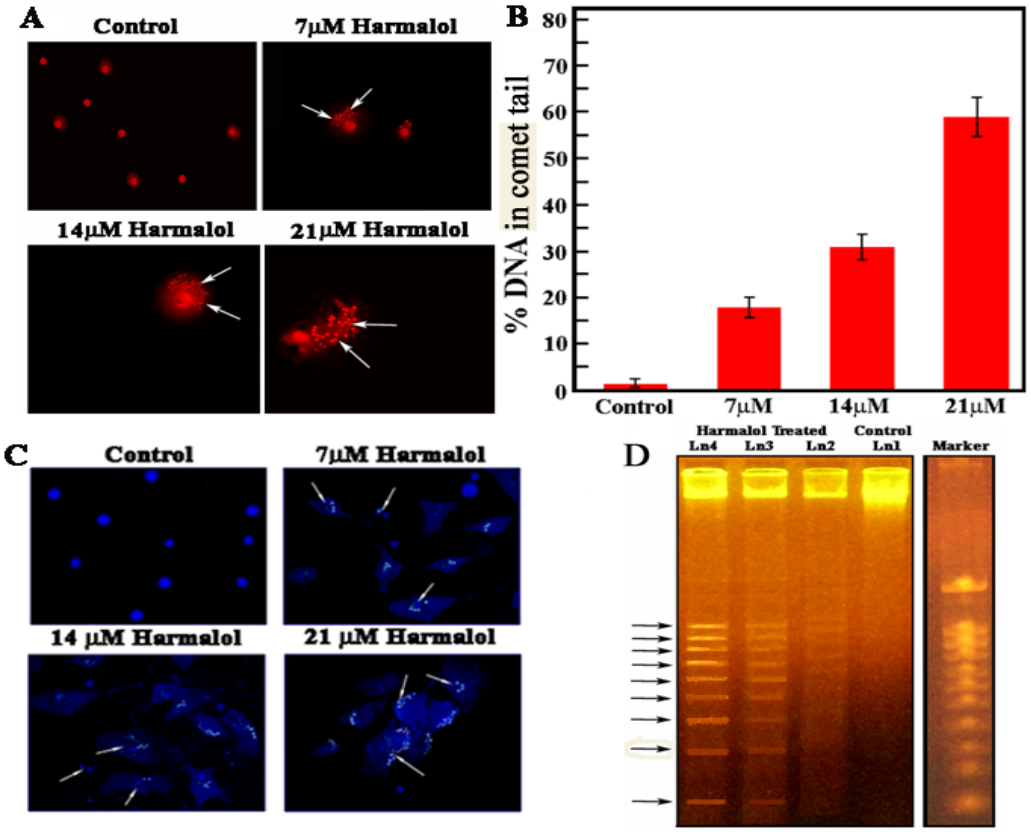

Fig. 2 (A) Comet assay showing detectable comet tails (marked with arrows) with increasing concentration of harmalol, indicative of DNA damage. (B) Bar graph representation of effect of harmalol treatment on% DNA damage of $HepG_2$ cell by comet assay using the software Casp. (C) Stained and fragmented nucleolous with DAPI as observed under a fluorescence microscope (200×). (D) Degradation of chromosomal DNA as DNA laddering formation during harmalol treatment at various concentrations

Treatment with harmalol, induced phosphatidylserine (PS) externalization in $HepG_2$ cells, which is again another remarkable characteristic of early stage of apoptosis. Fig. 3 (A) shows the quantitative results of bivariate FITC-Annexin V/PI FCM of $HepG_2$ cells after treatment with harmalol for different concentrations (at GI_{25}, GI_{50} and GI_{75} concentrations of 7, 14 and 21 μM respectively). The lower left quadrant of the cytograms shows the viable cells, which exclude PI and are negative for FITC-Annexin V binding because of intact cytoplasmic membrane. The upper right quadrant represents the non-viable, necrotic cells, positive for FITC-Annexin V binding and showing PI uptake. Further, the lower right quadrant represents the apoptotic cells, FITC-Annexin V positive and PI negative, demonstrating Annexin V binding to PS and cytoplasmic membrane integrity. The $FITC^+/PI^-$ apoptotic cell population increased gradually from 4.3±0.5% of control to 12.8±1.3% after treatment with 7 μM, 29.3±1.6% after treatment with 14 μM and 47.3±2.1% after treatment with 21 μM. On the other hand, FITC+/ PI+ necrotic cell population was increased from 1.1±0.4% to 4.4±1.4% after 48 h of treatment. To further validate the ability of harmalol on inducing apoptosis in $HepG_2$ cells, we performed a cellular functional assay. JC-1 probe, a voltage sensitive fluorescent cationic dye, exhibits membrane potential dependent accumulation in mitochondria, indicated by a fluorescence emission shift from red to green. The dye detects normal polarized mitochondria as red color and depolarized mitochondrial membranes as green color. The exposure of harmalol at GI_{50} to $HepG_2$ cells caused remarkable loss of mitochondrial membrane potential, hence the fluorescence shifted from red to green as the membrane potential (Ψm) decreased (Fig. 3 (B)).

Cell cycle analyses of harmalol-treated $HepG_2$ cells were further analysed by using PI staining, and the cell distributions were expressed among subG0-/G1, G0-/G1, S and G2/M phases. Time kinetics study of harmalol-treated cells indicated increasing accumulation of cells at subG0/G1-phase. The percentages of sub G0/G1 arrest were 3.33±0.6%, 10.42±1.0% and 17.14± 1.2% respectively, after 7, 14 and 21 μM treatment for 48 h in $HepG_2$ cells (Fig. 4 (A)). Cells were exposed to GI_{50} concentration of harmalol for 6, 12, 24 and 48 h and analyzed for the presence of ROS using ROS sensitive probe DCFH-DA (Fig. 4 (B)). ROS levels were found to be elevated during the course of treatment in the cell lines. The mean fluorescent intensity changed from 20.93 (control) to 22.68, 37.85, 74.05 and 89.49 after 6, 12, 24 and 48 h treatment, respectively (inset of Fig. 4 (B), upper panel). ROS intensity increased nearly about four folds from their control till 48 h treatment of harmalol. Moreover, pre-incubation with NAC (N-acetyl-L-cysteine) also inhibited the growth inhibitory role

of harmalol (inset of Fig. 4 (B), upper panel). From this study it may be inferred that harmalol induced death in $HepG_2$ cell precede via ROS mediated pathway. Detection of harmalol induced apoptosis in $HepG_2$ cells were further confirmed by RT-PCR data revealing that unlike in untreated cells, harmalol treatment resulted in activation of Caspase 3 and increase in expression of p53 in a dose dependent manner (inset of Fig. 4 (C)).

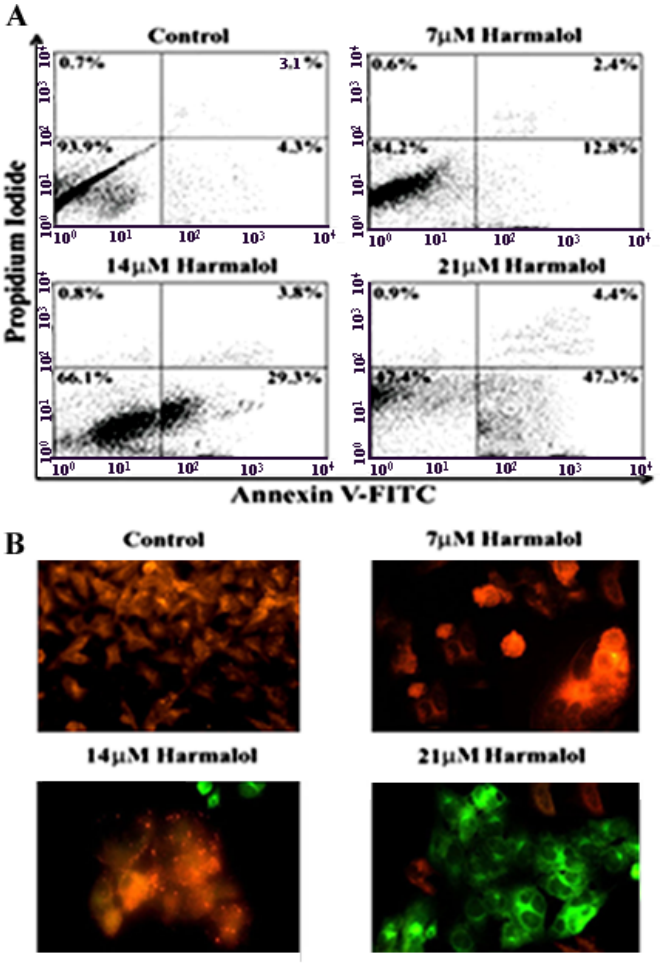

Fig. 3 (A) Contour diagram of FITC-Annexin V/PI flow cytometry of $HepG_2$ cells after 48 h of incubation at untreated, GI_{25}, GI_{50} and GI_{75} concentrations of 0, 7, 14 and 21 μM respectively. (B) Dose-dependent effect of harmalol upon changes of mitochondrial membrane potential using JC-1 stain as viewed under fluorescence microscope (200×)

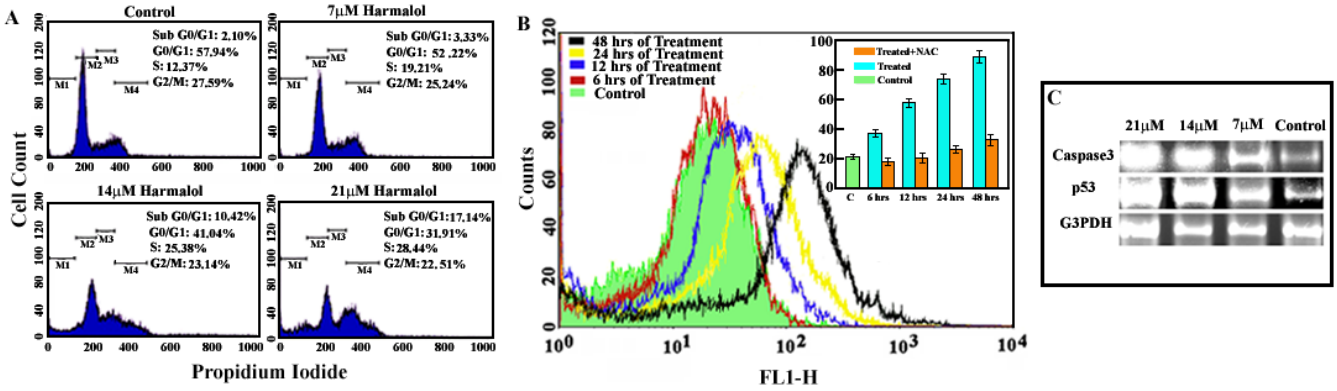

Fig. 4 (A) Cell cycle analysis of harmalol treated $HepG_2$ cells at 7 μM, 14 μM and 21 μM for 48h of incubation. Data are representative of three independent experiments, and the means are significant compared with their control ($P< 0.05$). (B) Harmalol induced ROS generation in $HepG_2$ cells. (inset) Percentage of growth inhibition in $HepG_2$ cells in presence of NAC. (C) RT-PCR analysis as conducted with cytosolic fraction of caspase 3 and p53 activation. GAPDH used as internal control for normalization of equal loading

B. Binding, Stabilization and Conformational Changes in DNA

Though the conformational changes associated with the binding of harmalol with CT-DNA was probed earlier by the authors through CD studies (5), but no quantitative data was reported from it. Both intrinsic (Fig. 5), as well as extrinsic, CD measurements of the DNA (inset of Fig. 5) on complexation with harmalol at pH 6.8 showed a regular and very prominent perturbation in molar ellipticity. The data from CD was used here to evaluate the binding phenomena as described by Zhong et al. [19]. The different spectra showed maximum at 278 nm and the change in the ellipticity of the different spectrum at 278 nm (θ_{278}) versus harmalol concentration was plotted (Fig. 6 (A)). The distance from the ordinate to the tangent at a given $\Delta\theta$ is equivalent to the concentration of the bound alkaloid (C_B) while the distance from the tangent to the curve gives the concentration of the free alkaloid (C_f). A Scatchard plot constructed from this data showed cooperative binding plotted (inset of Fig. 6 (A)) from which the cooperative binding affinity ($K'\omega$) of 4.65± 0.7 × 10^5 M^{-1}, an n value of 4.16 and a cooperativity factor (ω) of 31 were deduced. These values are presented in Table III, which are in good agreement to the values obtained earlier from absorption and fluorescence studies [5].

Apart from giving information about the stabilization of the polymer, thermal melting of DNA–drug complexes, elucidated the binding parameters with enthalpy data from DSC. DSC melting temperature of CT-DNA plotted (Fig. 6 (B)) under similar conditions were in complete agreement with the optical melting data with a stabilization of ΔT_m 8 °C plotted (inset of Fig. 6 (B)) and the values of ΔH_m evaluated from the DSC thermograms are presented in Table I. It may be noted that in the present study, the melting experiment was performed at saturating D/P of 0.7 and the data was used to calculate the binding constant of harmalol to CT-DNA using the equation derived by McGhee [20]:

$$1/T_m^o - 1/T_m = (R/\Delta H_m) \ln (1 + K_{Tm} L)^{1/n} \quad (1)$$

where $T_m°$ is the optical melting temperature of DNA alone, T_m is the melting temperature in presence of saturating amounts of the drug, ΔH_m is the enthalpy of DNA melting obtained by DSC experiment, R is the gas constant, K_{Tm} is the drug binding constant at T_m, L is the free drug concentration, and n is the size of the drug-binding site. The calculated apparent binding constant at the melting temperature can be extrapolated to a reference temperature using the standard relationship:

$$\ln (K/K_{Tm}) = -(\Delta H_b/R)(1/T - 1/T_m) \quad (2)$$

where K is the drug binding constant at the reference temperature T (in Kelvin) and ΔH_b, the binding enthalpy that was directly determined from the isothermal titration calorimetry experiment done earlier [5]. The binding constant value obtained by this methodology is in reasonable concordance with that evaluated directly from ITC and other spectroscopic techniques reported earlier [5].

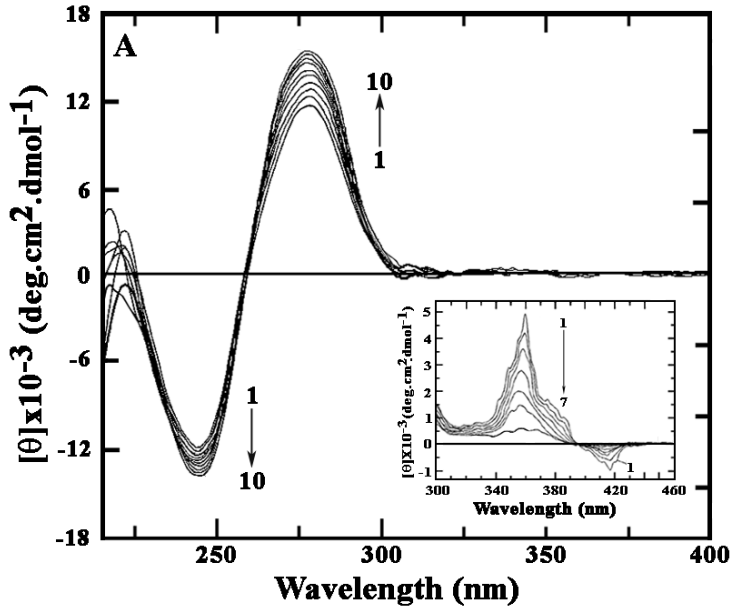

Fig. 5 Intrinsic CD spectra resulting from the interaction of harmalol, with CT DNA. Curves (1–10) denotes DNA (65 μM,) treated with 0, 1.2, 2.0, 4.0, 8.0, 12.0, 16.0, 25.0, 34.0 and 45.3 μM of harmalol. (Inset, lower panel): Extrinsic CD spectra of harmalol (50 μM) treated with CT DNA of 500, 400, 200, 125, 75, 50 and 25 μM of concentrations as shown by curves (1–7)

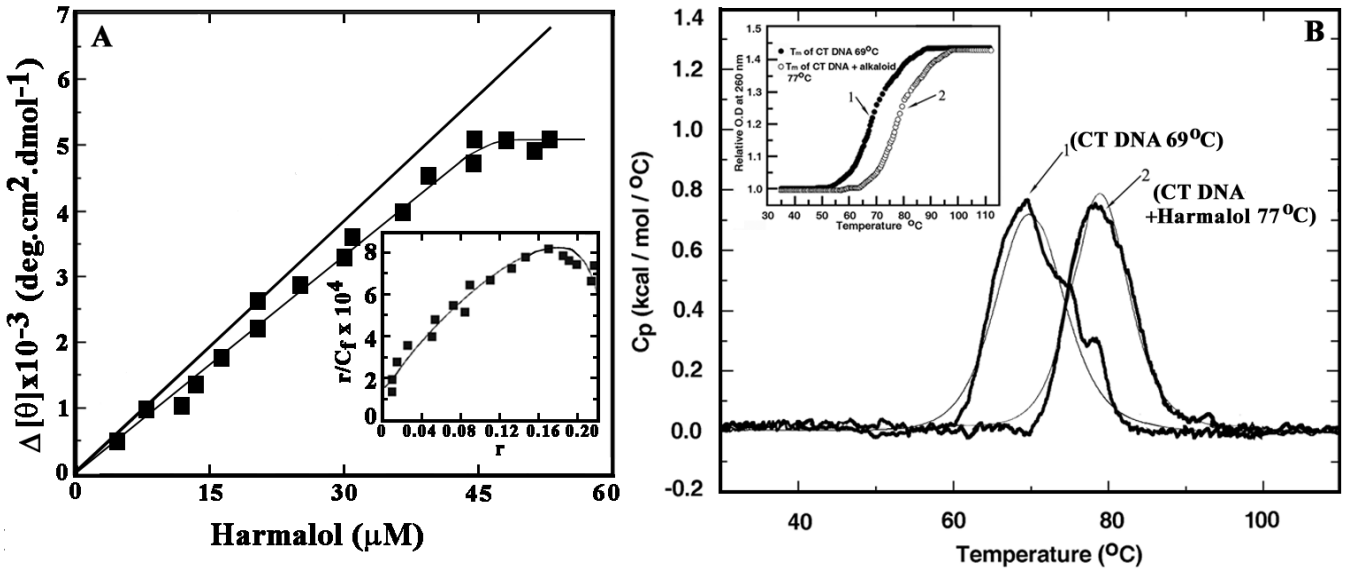

Fig. 6 (A) Plot of molar ellipticity (θ) change of CT DNA on harmalol titration versus harmalol concentration in the same buffer. Inset: Scatchard plot for CT DNA–harmalol complexation. (B) DSC thermogram of CT DNA (curve 1) and its complexation with harmalol (curve 2). Inset: Optical thermal melting profile of the same polymer

IV. Discussions

Present investigation has deciphered harmalol induced cytotoxicity and apoptosis in $HepG_2$ cells, along with its binding ability and stabilization with DNA. Previously also, harmalol has been reported to be very effective on dioxin mediated induction of CYP1A1 in human hepatoma $HepG_2$ cells and reported to have antimutagenic and antigenotoxic effects because of the antioxidant properties [21]-[23].

Any drug with a good anti-cancer potential should have the ability to induce apoptosis in cancer cells and is considered as one of the hallmark features of the anti-cancer drug [24]. Apoptosis, which is a complex set of multi branched, multistep pathways with many checks and balances, is elucidated by a large number of assays that are devised to detect and count apoptotic cells. Furthermore, many features of apoptosis and necrosis can overlap, and therefore it is important to employ two or more specific assays to confirm that cell death is occurring via apoptosis only [24]. Apoptosis triggered by various stimuli is characterized by a series of distinct biochemical and morphological changes [25]. $HepG_2$ cells exposed to different doses of harmalol at GI_{25}, GI_{50} and GI_{75} concentrations of 7, 14 and 21 μM respectively, also showed several such apoptotic characteristic like DNA ladder formation, chromatin condensation, nucloelous fragmentation, cytoplasmic blebbing, formation of comet tails, alteration of membrane structure, loss of mitochondrial membrane potential and formation of phagolysosome, all of which confirmed the progression of the cells towards apoptosis. Furthermore, FITC-Annexin V/PI FCM and LDH assay supported higher percentage of apoptosis comparative to negligible percentage of necrosis in harmalol treated $HepG_2$ cells. Our result further complimented with ROS dependent cytotoxicity that increased nearly 4 folds from their control until 48 h. ROS generation, induced by various anti-cancer agents, plays key role in apoptosis [24]. An elevated ROS level in HepG2 cells induced by harmalol is associated with increasing p53 induction and activation of caspase-3.

Apoptosis is specifically known to be intimately associated with the alteration of nucleic acid structure, function or stability. A new generation of agents that target nucleic acids associated processes, are anticipated to be far more specific and effective in cancer therapeutics. Our results too supported these views in CT DNA. One of the later steps in apoptosis is ultimately the DNA fragmentation, a process which results from the activation of endonucleases during the apoptotic programme [26]. Here we had opted for two methods, *viz*. CD and DSC to study the interaction, conformational changes, and analysis of binding constant and stabilization of the CT DNA with harmalol. The increased magnitudes of the DNA CD bands are speculative of intercalative ligand-DNA complexation and also signify that harmalol induces conformational changes in the DNA. The extrinsic CD where DNA does not have any contribution and results from the nondegenerative coupling of the ligand chromophore with the transition moments of the adjacent base pairs of the DNA (some chiral electronic interactions π-π* at the binding site) there by giving information about the orientation of the chromophore inside the helical organization. Furthermore, thermal melting data from DSC of CT DNA–harmalol complexes, apart from highlighting the stabilization of the DNA, is an important tool that elucidated the binding parameters. The binding parameter obtained from DSC melting data was in good agreement with the CD data. The ultimate objective of all such studies are eventually to develop more effective chemotherapeutic drugs from the natural product with enhanced efficiency and lower toxicity that can be targeted effectively in the future to cancer affected organ for better therapeutic applications.

In conclusion, our results demonstrated harmalol as a plausible effective alkaloid for inducing ROS dependent, caspase activated apoptosis in the human liver cancer cell line, $HepG_2$ and furthermore, shows binding, stabilization and conformational changes in DNA. Hence, this research work will enhance harmalol as a potential chemo preventive agent against liver cancer and will enable the researchers to develop a better, potent beta carboline- indole derivative for future biomedical applications.

TABLE I
OLIGO-PRIMER SEQUENCES FOR RT-PCR. OLIGOS SHIPPED IN LYOPHILLIZED FORM COMPANY: XCELRIS

Name of the gene	Sequence of primer
Casepase3	Forward-5'-AGGGGTCATTTATGGGACA-3'
	Reverse-5'-TACACGGGATCTGTTTCTTTG-3'
P53	Forward-5'-GGAAATTTGTATCCCGAGTATCTG-3'
	Reverse-5'-GTCTTCCAGTGTGATGATGGTAA-3'
G3PDH	Forward-5'-ATGGGGAAGGTGAAGGTCGG-3'
	Reverse-5'-GGATGCTAAGCAGTTGGT-3'

TABLE II
CALCULATION OF% DNA DAMAGE IN COMET ASSAY ANALYSIS[A]

GI value with harmalol concentration in μM	% DNA Damage
0	1.6±0.9
25 (7 μM)	18±2.2
50 (14 μM)	31±2.8
75 (21 μM)	59±4.3

[a]Average of three independent experiments.

TABLE III
CALCULATION OF BINDING CONSTANT AND MELTING TEMPERATURE OF CT DNA AND ITS COMPLEXATION WITH HARMALOL AT SATURATION D/P RATIO OF 0.7 IN 15 MM CITRATE–PHOSPHATE (CP) BUFFER OF PH 6.8.

CD method	$K' = 1.5\pm 0.2 \times 10^4$; $\omega = 31$; $K' \times \omega = 4.65\pm 0.7 \times 10^5$; n = 4.16				
DSC	$T_m°$ (°C)	T_m (°C)	ΔT_m (°C)	ΔH_m (kcal/mol)	K_a ($\times 10^5$ M^{-1})
	69	77	8	8.19±0.9	$5.10 \pm 0.6 \times 10^5$

Average of three independent experiments.

ACKNOWLEDGMENT

KB is indebted to the Council of Scientific and Industrial Research (CSIR), Government of India for the financial support (Ref. No. 37 (1538)/12/EMR-II). Author is also thankful to DST-PURSE and PRG-2015-16, University of Kalyani.

REFERENCES

[1] M. F. Roberts, and M. Wink, in: M. F. Roberts, M. Wink, editors, Ecology and medicinal applications, alkaloids, New York, London: Plenum Press; Biochemistry (1998) 1.
[2] K. Bhadra, G. Suresh Kumar, Therapeutic potential of nucleic acid binding isoquinoline alkaloids: Binding aspects and implications for drug design, Med. Res. Rev. 31 (2011) 821-862.
[3] R. Ali, Z. Mirza, G. M. Ashraf, M. A. Kamal, S. A. Ansari, G. A. Damanhouri, A. M. Abuzenadah, A. G. Chaudhary, I. A. Sheikh, New anticancer agents: recent developments in tumor therapy, Anticancer Res. 32 (2012) 2999-3005.
[4] M. Moudi, R. Go, C. Y. S. Yien, M. Nazre, Vinca Alkaloids, Int. J. Prev. Med. 4 (2013) 1231–1235.
[5] S. Sarkar, K. Bhadra, Binding of alkaloid harmalol to DNA: photophysical and calorimetric approaches, J. Photochem. Photobiol. B. 130 (2014) 272-80.
[6] S. Sarkar, P. Pandya, K. Bhadra, Sequence specific binding of beta carboline alkaloid harmalol with deoxyribonucleotides: Binding heterogeneity, conformational, thermodynamic and cytotoxic aspects, Plos One (2014) DOI: 10.1371/journal.pone.0108022.
[7] P. Bhattacharjee, S. Sarkar, P. Pandya, K. Bhadra, Targeting different RNA motifs by beta carboline alkaloid, harmalol: A comparative photophysical, calorimetric and molecular docking approach, J. Biomol. Struct. Dyn. (2015) DOI:10.1080/07391102.2015.1126694.
[8] D.H. Aarons, G.V. Rossi, R.F. Orzechowski, Cardiovascular actions of three harmala alkaloids: harmine, harmaline and harmalol, J. Pharm. Sci. 66 (1977) 1244–1248.
[9] M. Mahmoudian, H. Jalilpour, P. Salehian, Toxicity of Peganum harmala: review and a case report, Iran J. Pharmacol. Therap. 1 (2002) 1–4.
[10] R. Cao, W. Peng, Z. Wang, A. Xu, β-Carboline alkaloids: biochemical and pharmacological functions, Curr. Med. Chem. 14 (2007) 479–500.
[11] T. Herraiz, Identification and occurrence of beta-carboline alkaloids in raisins and inhibition of monoamine oxidase (MAO), J. Agric. Food Chem. 55(2007) 8534–8540.
[12] T. Uezono, W. Maruyama, K. Matsubara, M. Naoi, K. Shimizu, O. Saito, Norharman an indoleamine-derived betacarboline, but not Trp-P-2, a gamma-carboline, induces apoptotic cell death in human neuroblantoma SH-SY5Y cells, J. Neural Transm. 108 (2001) 943-953.
[13] F. Lamchouri, M. Zemzami, A. Jossang, A. Settaf, Z. H. Israili, B. Lyoussi, Cytotoxicity of alkaloids isolated from Peganum harmala seeds, Pak. J. Pharm. Sci. 26 (2013) 699-706.
[14] D.L. Bemis, J.L. Capodice, P. Gorroochurn, A.E. Katz, R. Buttyan, Anti-prostate cancer activity of a beta-carboline alkaloid enriched extract from Rauwolfia vomitoria, Int. J. Oncol. 29 (2006) 1065-1073.
[15] S. Chatterjee, S. Mallick, F. Buzzetti, G. Fiorillo, T. M. Syeda, P. Lombardi, K. Das Saha, G. Suresh Kumar, New 13-pyridinealkyl berberine analoguesintercalate to DNA and induce apoptosis in $HepG_2$ and MCF-7 cells through ROS mediated p53 dependent pathway: biophysical, biochemical and molecular modeling studies, RSC Advances. 5 (2015) 90632-90644.
[16] S. Mallick, P. Ghosh, S. K. Samanta, S. Kinra, B. C. Pal, A. Gomes, J. R. Vedasiromoni, Corchorusin-D, a saikosaponin-like compound isolated from *Corchorus acutangulus* Lam., targets mitochondrial apoptotic pathways in leukemic cell lines (HL-60 and U937), Cancer Chemother. Pharmacol., 66 (2010) 709–719.
[17] N. Morley, A. Rapp, H. Dittmar, L. Salter, D. Gould, K.O. Greulich, A. Curnow, UVA-induced apoptosis studied by the new apo/necro-Comet-assay which distinguishes viable, apoptotic and necrotic cells, Mutagenesis 21 (2006) 105–114.
[18] K. Bhadra, M. Maiti, G. Suresh Kumar, Thermodynamics of the binding of cytotoxic protoberberine molecule coralyne to deoxyribonucleic acids, Biochim. Biophys. Acta 1780 (2008) 298-306.
[19] W. Zhong, J.S. Yu, Y. Liang, K. Fan, L. Lai, Chlorobenzylidine-calf thymus DNA interaction II: circular dichroism and nuclear magnetic resonance studies, Spectrochim. Acta A. 60 (2004) 2985–2992.
[20] J.D. McGhee, Theoretical calculations of helix-coil transition of DNA in the presence of large, cooperatively binding ligands, Biopolymers 15 (1976) 1345–1375.
[21] A. M. El Gendy, A. A. Soshilov, M. S. Denison, O. S. El-Kadi, Transcriptional and posttranslational inhibition of dioxin-mediated induction of CYP1A1 by harmine and harmol, Toxicol Lett. 208 (2012) 51–61.
[22] J. N. Picada, K. V. C. L. da Silva, E. D. Erdtmann, A. T. Henriques, J.A.P. Henriques, Genotoxic effects of structurally related β-carboline alkaloids, Mutat. Res. 379 (1997) 135–149.
[23] D. J. Moura, M. F. Richter, J. M. Boeira, J. A. P. Henriques, J. Saffi, Antioxidant properties of β-carboline alkaloids are related to their antimutagenic and antigenotoxic activities, Mutagenesis 22 (2007) 293–302.
[24] S. Elmore, Apoptosis: A Review of Programmed Cell Death, Toxicol. Pathol. 35 (2007) 495–516.
[25] A. H. Wyllie, The genetic regulation of apoptosis, Curr. Opin. Genet. Dev. 5 (1995) 97–104.
[26] J. Das, S. Das, A. Samadder, K. Bhadra, A. R. Khuda-Bukhsh, Poly (lactide-co-glycolide) encapsulated extract of *Phytolacca decandra* demonstrates better intervention against induced lung adenocarcinoma in mice and on A549 cells, European J. of Pharma. Sci. 47 (2012) 313–324.